REPORT NO.
UCB/SEMM-95/10

STRUCTURAL ENGINEERING
MECHANICS AND MATERIALS

# ACCURACY AND STABILITY FOR INTEGRATION OF JAUMANN STRESS RATE EQUATIONS IN SPINNING BODIES

BY

SANJAY GOVINDJEE

AUGUST 1995

DEPARTMENT OF CIVIL ENGINEERING
UNIVERSITY OF CALIFORNIA
BERKELEY, CALIFORNIA

# *Accuracy and Stability for Integration of Jaumann Stress Rate Equations in Spinning Bodies*

SANJAY GOVINDJEE

Department of Civil Engineering
University of California
Berkeley, CA 94720

## § Abstract

In this paper, several algorithms for the integration of the Jaumann stress rate are analyzed. Emphasis is placed upon accuracy and stability of standard algorithms available in commercial and government finite element codes in addition to several other proposals available in the literature. The analysis is primarily concerned with spinning bodies and reveals that a commonally used algorithm is unconditionally unstable and only first order objective in the presence of rotations. Other proposals are shown to have better accuracy and stability properties. Lastly, it is shown by example that even consistent and unconditionally stable integration of hypoelastic constitution does not necessarily yield globally stable finite element simulations.

## §1. Introduction

Large-deformation problems in solid mechanics are typically solved via numerical techniques such as the finite element method. Many finite element codes (see e.g. [1,4]) rely upon the objective Jaumann rate form of the constitutive relation (a form of hypoelasticity). This is especially true for programs that utilize explicit integration of the equations of motion. While this form of the constitutive relation is known to exhibit unusual behavior in problems involving very large shear deformations [2,3], it is nonetheless a popular choice because of the simplicity of the kinematic quantities involved in its definition.

In this paper, the interest is in the utilization of this framework for the dynamic simulation of the motion of spinning bodies and other motions involving large rigid-body rotational components. Common examples would include rotating machinery or tumbling bodies. In the classical implementation of the Jaumann rate form of the constitution, the rate of change of the stress is approximated via a finite difference scheme. The classical method will be shown to be (1) only first order objective (though the Jaumann stress rate itself is known to be objective) and (2) unconditionally unstable in the presence of rotations. The inaccuracy generated by the first order objective algorithm and its unconditional instability leads to a premature generation of global instability in the time stepping simulation of the problems of interest when the time duration is sufficiently long. In this paper, an alternative integration scheme for the Jaumann constitutive relation is presented that is second order objective and more stable than the common first order objective algorithm. This combination of improvements appreciably delays the global instability mentioned above.

For comparison purposes, several fully objective unconditionally stable integration schemes are also analyzed. These include the Hughes-Winget method [5,7], the exponential map algorithm [5], and a hyperelastic formulation. It is noted, however, that these algorithms involve more expensive kinematic computations. Nonetheless all the algorithms, except for the hyperelastic formulation, involve the use of kinematic quantities that are used in the standard finite element framework of explicit codes with Jaumann rate equations. The added cost of the second order algorithm is the least expensive in comparison to the other options. It is also noted that the algorithms presented are applicable to both 2 and 3 dimensional problems.

The remainder of the paper is organized as follows: In section 2, the conventional global and constitution level algorithms for explicit finite element calculations are briefly reviewed. In section 3, the standard constitution algorithm for the Jaumann stress rate form will be given an interpretation that allows for a natural extension to higher order accuracy with minimal cost. Section 4 analyzes the five algorithms for accuracy and stability during rigid-body motion. Lastly, Section 5 presents some illustrative examples, followed by a few concluding remarks in Section 6.

## §2. Conventional Algorithmic Framework

*Global framework*

The basic finite element equations after spatial discretization are of the following form

$$\boldsymbol{M}\boldsymbol{a} = \boldsymbol{P} - \boldsymbol{F}\,, \tag{2.1}$$

where $\boldsymbol{M}$ is a mass matrix‡, $\boldsymbol{a}$ is a vector of nodal accelerations, $\boldsymbol{P}$ is a vector of external nodal loads, and $\boldsymbol{F}$ is the internal force vector. The internal force vector is further given by the expression

$$\boldsymbol{F} = \int_V \boldsymbol{B}^T\boldsymbol{\sigma}\,, \tag{2.2}$$

where $V$ is the current placement of the body of interest, $\boldsymbol{B}$ is the matrix of shape function derivatives with respect to the current configuration of the body, the superscript $T$ indicates the transpose operation, and $\boldsymbol{\sigma}$ is the Cauchy stress. The constitutive response of the body is, for our purposes, given by the Jaumann stress rate form

$$\overset{\nabla}{\boldsymbol{\sigma}} = \mathbb{C}\colon\boldsymbol{d}\,, \tag{2.3}$$

where $\mathbb{C}$ is a constant rank-4 constitutive tensor, $\boldsymbol{d}$ is the symmetric part of the spatial velocity gradient (rate of deformation tensor), the $(:)$ indicates double contraction, and

$$\overset{\nabla}{\boldsymbol{\sigma}} = \dot{\boldsymbol{\sigma}} - \boldsymbol{\sigma}\boldsymbol{\Omega} + \boldsymbol{\Omega}\boldsymbol{\sigma}\,. \tag{2.4}$$

Here, $\boldsymbol{\Omega}$ is the transpose of the skew part of the spatial velocity gradient and a superposed dot $(\dot{})$ indicates (material) time differentiation.

Key to the utilization of this framework is a time integration method. Explicit codes typically make use of the Central Difference algorithm, or equivalently the Newmark algorithm with $\beta = 0$ and $\gamma = \frac{1}{2}$, where $\beta$ and $\gamma$ are the Newmark parameters; see e.g. [6] for an elementary presentation. The essential feature of this framework is a prescription for the advancement of a solution $(\boldsymbol{u}_n, \boldsymbol{v}_n, \boldsymbol{a}_n)$ at time $t_n$ to time $t_{n+1} = t_n + \Delta t$, where $\Delta t > 0$ is a time step increment, $\boldsymbol{u}_n$ is a vector of nodal displacements at time $t_n$, $\boldsymbol{v}_n$ is a vector of nodal velocities at time $t_n$, and $\boldsymbol{a}_n$ is a vector of nodal accelerations at time $t_n$*. Assuming the solution at time $t_n$ is known, the solution is advanced to $t_{n+1}$ via the following relations:

$$\boldsymbol{u}_{n+1} = \boldsymbol{u}_n + \Delta t\boldsymbol{v}_n + \frac{\Delta t^2}{2}\boldsymbol{a}_n\,, \tag{2.5}$$

$$\boldsymbol{a}_{n+1} = \boldsymbol{M}^{-1}(\boldsymbol{P}_{n+1} - \boldsymbol{F}_{n+1})\,, \tag{2.6}$$

and

$$\boldsymbol{v}_{n+1} = \boldsymbol{v}_n + \frac{\Delta t}{2}(\boldsymbol{a}_n + \boldsymbol{a}_{n+1})\,. \tag{2.7}$$

---

‡ In typical explicit algorithms the mass matrix is lumped in some fashion (diagonalized).

* Here and throughout the manuscript, subscript $n$'s and $n+1$'s denote quantities at time $t_n$ and $t_{n+1}$, respectively.

*Stress integration*

In order to use the above advancement procedure one needs an algorithm for the computation of $\boldsymbol{\sigma}_{n+1}$. This is conventionally computed via the integration algorithm (denoted henceforth as ALGO1):

$$\boldsymbol{\sigma}_{n+1} = \boldsymbol{\sigma}_n + \dot{\boldsymbol{\sigma}}_{n+1/2}\Delta t\,, \tag{2.8}$$

where

$$\dot{\boldsymbol{\sigma}}_{n+1/2} = \overset{\triangledown}{\boldsymbol{\sigma}}_{n+1/2} + \boldsymbol{\sigma}_n\boldsymbol{\Omega}_{n+1/2} - \boldsymbol{\Omega}_{n+1/2}\boldsymbol{\sigma}_n \tag{2.9}$$

and

$$\overset{\triangledown}{\boldsymbol{\sigma}}_{n+1/2} = \mathbb{C}\colon \boldsymbol{d}_{n+1/2}\,. \tag{2.10}$$

The use of (2.9) and (2.10) requires knowledge of the half-step velocities and geometry. These are computed as

$$\boldsymbol{v}_{n+1/2} = \boldsymbol{v}_n + \frac{\Delta t}{2}\boldsymbol{a}_n \tag{2.11}$$

and

$$\boldsymbol{x}_{n+1/2} = \boldsymbol{X} + \boldsymbol{u}_n + \frac{\Delta t}{2}\boldsymbol{v}_{n+1/2}\,, \tag{2.12}$$

where $\boldsymbol{X}$ is the vector of initial nodal positions and $\boldsymbol{x}_{n+1/2}$ is the vector of half-step nodal positions. In this setting,

$$\boldsymbol{d}_{n+1/2} = \tfrac{1}{2}\left[\frac{\partial \boldsymbol{v}_{n+1/2}}{\partial \boldsymbol{x}_{n+1/2}} + \left(\frac{\partial \boldsymbol{v}_{n+1/2}}{\partial \boldsymbol{x}_{n+1/2}}\right)^T\right] \tag{2.13}$$

and

$$\boldsymbol{\Omega}_{n+1/2} = -\tfrac{1}{2}\left[\frac{\partial \boldsymbol{v}_{n+1/2}}{\partial \boldsymbol{x}_{n+1/2}} - \left(\frac{\partial \boldsymbol{v}_{n+1/2}}{\partial \boldsymbol{x}_{n+1/2}}\right)^T\right]. \tag{2.14}$$

Note that while ALGO1 is similar in form to a mid-point integration rule, it is in fact a mixture of a mid-point and a forward Euler integration rule, as will be seen more clearly in §4.

**Remark 2.1.**

Often the additional calculation of the half-step geometry is not performed and velocity gradients at time $t_{n+1/2}$ are computed by differentiating the half-step velocities with respect to the full-step geometry ($\boldsymbol{X} + \boldsymbol{u}_{n+1}$). This, however, introduces additional error into the stress integration algorithm and its use is avoided here. □

## §3. Interpretation and Alternative Algorithms

*Rigid motion interpretation*

Consider a motion that involves only a rigid-body rotation between time $t_n$ and $t_{n+1}$ and is described by the constant rotation tensor $\boldsymbol{Q}$. If one assumes a perfect kinematical calculation, then $\boldsymbol{d} = 0$ and the principle of frame invariance (objectivity) dictates that $\boldsymbol{\sigma}_{n+1} = \boldsymbol{Q}\boldsymbol{\sigma}_n\boldsymbol{Q}^T$. The rotation tensor may be expanded in a series in terms of a skew-symmetric tensor $\boldsymbol{\omega}$ as

$$\boldsymbol{Q} = \exp[-\boldsymbol{\omega}] = \boldsymbol{1} - \boldsymbol{\omega} + O(\|\boldsymbol{\omega}\|^2)\,, \tag{3.1}$$

where $\|\boldsymbol{\omega}\| = \sqrt{\frac{1}{2}\boldsymbol{\omega}:\boldsymbol{\omega}}$ for $\boldsymbol{\omega} \in so(3)$ and $O(x)$ for $x \in \mathbb{R}$ denotes conventional order notation (i.e. $\lim_{x\to 0} O(x)/x = \text{constant}$). Thus, one has that

$$\boldsymbol{\sigma}_{n+1} = \boldsymbol{\sigma}_n + \boldsymbol{\sigma}_n\boldsymbol{\omega} - \boldsymbol{\omega}\boldsymbol{\sigma}_n + O(\|\boldsymbol{\omega}\|^2)\,. \tag{3.2}$$

If one examines ALGO1 and notes that $\boldsymbol{d}_{n+1/2} = 0$ for the motion currently under consideration, then one has the result that

$$\boldsymbol{\sigma}_{n+1} = \boldsymbol{\sigma}_n + \boldsymbol{\sigma}_n(\boldsymbol{\Omega}_{n+1/2}\Delta t) - (\boldsymbol{\Omega}_{n+1/2}\Delta t)\boldsymbol{\sigma}_n\,. \tag{3.3}$$

A comparison of (3.2) and (3.3) results in the following interpretation of the stress integration algorithm after identifying $\boldsymbol{\omega}$ with $\boldsymbol{\Omega}_{n+1/2}\Delta t$:

> *The last two terms on the right-hand-side of (2.9) account for rigid-body motion and produce an algorithm that is first order objective; i.e. the objectivity error is* $O(\|\boldsymbol{\Omega}_{n+1/2}\Delta t\|^2)$.

*Natural extension to higher order*

The method of interpreting the stress integration algorithm provides for a natural extension of the algorithm to higher order. This is achieved by expanding the expression for the incremental rotation tensor over a time step in higher powers of $\boldsymbol{\Omega}_{n+1/2}\Delta t$. By keeping terms to second order,

$$\boldsymbol{Q} = \exp[-\boldsymbol{\Omega}_{n+1/2}\Delta t] \approx \boldsymbol{1} - \boldsymbol{\Omega}_{n+1/2}\Delta t + \tfrac{1}{2}\boldsymbol{\Omega}^2_{n+1/2}\Delta t^2\,. \tag{3.4}$$

Using this expression and $\boldsymbol{\sigma}_{n+1} = \boldsymbol{Q}\boldsymbol{\sigma}_n\boldsymbol{Q}^T$, one can generate a replacement for the last two terms on the right-hand-side of (2.9). This leads to the following replacement for (2.9):

$$\begin{aligned}\dot{\boldsymbol{\sigma}}_{n+1/2} = \overset{\triangledown}{\boldsymbol{\sigma}}_{n+1/2} &+ \boldsymbol{\sigma}_n\boldsymbol{\Omega}_{n+1/2} - \boldsymbol{\Omega}_{n+1/2}\boldsymbol{\sigma}_n \\ &+ \tfrac{1}{2}\Delta t\left(\boldsymbol{\sigma}_n\boldsymbol{\Omega}^2_{n+1/2} - 2\boldsymbol{\Omega}_{n+1/2}\boldsymbol{\sigma}_n\boldsymbol{\Omega}_{n+1/2} + \boldsymbol{\Omega}^2_{n+1/2}\boldsymbol{\sigma}_n\right)\,.\end{aligned} \tag{3.5}$$

Eq. (3.5) together with (2.8) and (2.10) will be referred to as ALGO2.

**Remark 3.1.**
In going from (3.4) to (3.5) terms of $O(\|\boldsymbol{\Omega}_{n+1/2}\Delta t\|^3)$ have been dropped. This new algorithm is termed second order objective since the objectivity error in the integration of the stress during a rigid-body motion is $O(\|\boldsymbol{\Omega}_{n+1/2}\Delta t\|^3)$. □

**Remark 3.2.**
Note that the new algorithm does not involve the use of any kinematic quantities that were not present in the original first order objective algorithm. In terms of costs, ALGO1 requires 15 multiplies and 18 additions to perform the rotational update of the stress. ALGO2 requires an additional 45 multiplies and 36 additions. While this cost may seem high, it is less than other proposals available in the literature [5,7,10]. □

*Alternative algorithms*

Two alternative algorithms that can be used in the same capacity as shown above are the Hughes-Winget algorithm [7] and the exponential map. For the exponential map, Rodrigues' formula [8, p.165] gives an expression for the rotation $\boldsymbol{Q}$ entirely in terms of the spin as:

$$\begin{aligned}\boldsymbol{Q}_{\rm exp} = \exp[-\boldsymbol{\Omega}_{n+1/2}\Delta t] = \boldsymbol{1} - \frac{\sin(\|\boldsymbol{\Omega}_{n+1/2}\Delta t\|)}{\|\boldsymbol{\Omega}_{n+1/2}\Delta t\|}\boldsymbol{\Omega}_{n+1/2}\Delta t \\ + \tfrac{1}{2}\left(\frac{\sin(\|\boldsymbol{\Omega}_{n+1/2}\Delta t\|/2)}{\|\boldsymbol{\Omega}_{n+1/2}\Delta t\|/2}\right)^2 (\boldsymbol{\Omega}_{n+1/2}\Delta t)^2 .\end{aligned} \tag{3.6}$$

The final algorithm being:

$$\boldsymbol{\sigma}_{n+1} = \Delta t\mathbb{C} : \boldsymbol{d}_{n+1/2} + \boldsymbol{Q}_{\rm exp}\boldsymbol{\sigma}_n\boldsymbol{Q}_{\rm exp}^T . \tag{3.7}$$

During an incrementally rigid-body motion this algorithm produces the exact answer.

**Remark 3.3.**
While the expression for the exponential map is given entirely in terms of $\boldsymbol{\Omega}$ as desired, it involves the costly evaluation of trigonometric functions. A re-parameterization known as the pseudo-vector form and intimately related to the Cayley transform can reduce the number of trigonometric function evaluations required from a sine and cosine evaluation to a single tangent evaluation [9]. Nonetheless, the cost remains high in comparison to ALGO1 and ALGO2. □

The Hughes-Winget algorithm may be written in the following form:

$$\boldsymbol{Q}_{\rm HW} = \boldsymbol{1} + \frac{2}{2 + \frac{1}{2}\|\boldsymbol{\Omega}_{n+1/2}\Delta t\|^2}\left[-\boldsymbol{\Omega}_{n+1/2}\Delta t + \tfrac{1}{2}(\boldsymbol{\Omega}_{n+1/2}\Delta t)^2\right] , \tag{3.8}$$

with

$$\boldsymbol{\sigma}_{n+1} = \Delta t \mathbb{C} : \boldsymbol{d}_{n+1/2} + \boldsymbol{Q}_{\text{HW}} \boldsymbol{\sigma}_n \boldsymbol{Q}_{\text{HW}}^T \,. \tag{3.9}$$

In Eq. (3.8), the following identities have been utilized in re-writing the original formula of Hughes and Winget:

$$\begin{aligned} (\mathbf{1} - \boldsymbol{\omega})^{-1} &= \sum_{k=0}^{\infty} \boldsymbol{\omega}^k \\ \boldsymbol{\omega}^3 &= -\boldsymbol{\omega} \|\boldsymbol{\omega}\|^2 \,, \end{aligned} \tag{3.10}$$

where $\boldsymbol{\omega} \in so(3)$. The series in Eq. $(3.10)_1$ is valid for $\|\boldsymbol{\omega}\| < 1$.

**Remark 3.4.**

Both $\boldsymbol{Q}_{\text{exp}}$ and $\boldsymbol{Q}_{\text{HW}}$ are elements of $SO(3)$ but differ from each other. ALGO1 and ALGO2 do not produce members of $SO(3)$. □

**Remark 3.5.**

One major detraction of the Hughes-Winget and exponential map algorithms when used in the explicit framework is their cost. While the rotation expressions are similar in form to Eq. (3.4), they are quite a bit more expensive in their application ($\boldsymbol{Q}\boldsymbol{\sigma}_n\boldsymbol{Q}^T$). This follows, since terms of order greater than $O(\|\boldsymbol{\Omega}_{n+1/2}\Delta t\|^2)$ are retained and not truncated as is done in Eq. (3.5). As will be seen in §5 this added expense yields several desirable properties but may be of limited use in practical calculations. □

As a last alternative, the Saint Venant-Kirchhoff hyperelastic model is considered. This model is introduced to allow a comparison of the hypoelastic model and its algorithmic approximations to a more theoretically sound constitution. The model can be written so that the Cauchy stress at any time is given as

$$\boldsymbol{\sigma} = \frac{1}{J} \boldsymbol{F} \boldsymbol{S} \boldsymbol{F}^T \,, \tag{3.11}$$

where $\boldsymbol{F}$ is the deformation gradient, $J = \det[\boldsymbol{F}]$ is the Jacobian, $\boldsymbol{S} = \mathbb{C}\colon \boldsymbol{E}$ is the 2nd Piola-Kirchhoff stress tensor, and $\boldsymbol{E} = \frac{1}{2}(\boldsymbol{F}^T\boldsymbol{F} - \mathbf{1})$ is the Green-Lagrange strain tensor. This model can also be utilized in an incremental form whereby

$$\boldsymbol{\sigma}_{n+1} = \frac{1}{J_{n+1}} \boldsymbol{F}_{n+1} \left( \boldsymbol{S}_n + \mathbb{C}\colon \Delta \boldsymbol{E} \right) \boldsymbol{F}_{n+1}^T \tag{3.12}$$

and $\Delta \boldsymbol{E} = \dot{\boldsymbol{E}}_{n+1/2} \Delta t = \boldsymbol{F}_{n+1/2}^T \boldsymbol{d}_{n+1/2} \boldsymbol{F}_{n+1/2} \Delta t$. For the purposes of the comparisons in §5, this incremental form has been utilized to (1) force a direct dependence of the algorithm on the half-step velocity gradients and (2) introduce an incremental evaluation of the Cauchy stress. These features are introduced here since they both appear in the hypoelastic algorithms. This provides a more even basis for comparison. Note that this is certainly not the most efficient form.

**Remark 3.6.**

Because the Saint Venant-Kirchhoff model is hyperelastic the work is zero in closed processes [11, §28] – as one intuitively expects. This can not be said in general for hypoelastic bodies. The primary detraction of the Saint Venant-Kirchhoff model is that it is not polyconvex and can attain a state of zero volume at finite energy. For the purposes at hand, this is not an issue of concern. □

## §4. Accuracy and Stability

In this section several measures of accuracy will be examined for the algorithms given in the §3 as will analyses of their stability.

*Stress invariant accuracy*

An analytic determination of the benefit of the second order objective algorithm can be easily made in 2-D. Consider a motion that is purely rotational over a single time step with rotation $\boldsymbol{Q} = \exp[-\boldsymbol{\Omega}\Delta t]$. In 2-D, one may write in a given basis that

$$\boldsymbol{\Omega} = \alpha \begin{bmatrix} 0 & 1 \\ -1 & 0 \end{bmatrix} \tag{4.1}$$

where $\alpha$ is a given real number. Application of ALGO2 produces the result (in the same basis) that

$$\begin{bmatrix} \sigma_{11} & \sigma_{12} \\ \sigma_{12} & \sigma_{22} \end{bmatrix}_{n+1} = \begin{bmatrix} \sigma_{11} & \sigma_{12} \\ \sigma_{12} & \sigma_{22} \end{bmatrix}_n + \alpha\Delta t \begin{bmatrix} 2\sigma_{12} & \sigma_{22}-\sigma_{11} \\ \sigma_{22}-\sigma_{11} & -2\sigma_{12} \end{bmatrix}_n + \alpha^2\Delta t^2 \begin{bmatrix} \sigma_{22}-\sigma_{11} & -2\sigma_{12} \\ -2\sigma_{12} & -\sigma_{22}+\sigma_{11} \end{bmatrix}_n \tag{4.2}$$

In (4.2) the first two terms represent the result obtained from the application of ALGO1 and the last term on the right-hand-side is the added correction from ALGO2.

As a measure of the performance of the two algorithms, consider that during an incrementally rigid-body motion the invariants of the stress tensor should remain constant – viz., the trace and determinant. For the trace, both algorithms produce exact results. For the determinant, however, the first order objective algorithm gives

$$\det[\boldsymbol{\sigma}_{n+1}] = \det[\boldsymbol{\sigma}_n] + \alpha^2\Delta t^2 \left(4\sigma_{12_n}^2 + (\sigma_{22_n} - \sigma_{11_n})^2\right) \tag{4.3}$$

and the second order objective algorithm gives

$$\det[\boldsymbol{\sigma}_{n+1}] = \det[\boldsymbol{\sigma}_n] - \alpha^4\Delta t^4 \left(4\sigma_{12_n}^2 + (\sigma_{22_n} - \sigma_{11_n})^2\right) . \tag{4.4}$$

**Remark 4.1.**

In terms of invariant accuracy in 2-D during rigid-body motion, ALGO2 produces a third order accurate integrator and the ALGO1 produces a first order accurate integrator. The determinant errors are identically zero only in the case when the stress state is purely spherical. □

**Remark 4.2.**

All three alternative algorithms produce identically zero error in the trace and determinant. For the Hughes-Winget and exponential map algorithms, this follows directly from the fact that $\boldsymbol{Q} \in SO(3)$ in both cases. Note that the result from the exponential map is the exact solution to this problem – as is the result obtained from the Saint Venant-Kirchhoff model. It is also noted that to obtain this zero error state the $\boldsymbol{Q}\boldsymbol{\sigma}_n\boldsymbol{Q}^T$ operation must be performed using an invariant preserving method as opposed to direct matrix multiplication which introduces errors from finite precision arithmetic. For instance in 2-D, one could first compute the normal stress $\sigma_{11_{n+1}}$ using matrix multiplication, compute the other normal stress via $\sigma_{22_{n+1}} = \text{tr}\,[\boldsymbol{\sigma}_n] - \sigma_{11_{n+1}}$, and finally compute the shear stress via $\sigma_{12_{n+1}} = \sqrt{-\det[\boldsymbol{\sigma}_n] + \sigma_{11_{n+1}}\sigma_{22_{n+1}}}$. The sign of the shear stress must be chosen carefully. Similar but slightly more complex techniques are also possible in 3-D. □

**Remark 4.3.**

Even though the Hughes-Winget algorithm does not generate invariant error, it does possess an orientational error; i.e. the principal axes of $\boldsymbol{\sigma}_{n+1}$ are misaligned with respect to the exact solution from the exponential map for rigid-body rotations. As a measure of this accuracy, one may consider the error tensor which is the difference between the Hughes-Winget rotation and the exponential map rotation:

$$\boldsymbol{e} = \boldsymbol{Q}_{\text{HW}} - \boldsymbol{Q}_{\text{exp}} = -\frac{1}{12}\boldsymbol{\Omega}\|\boldsymbol{\Omega}\|^2 + O(\|\boldsymbol{\Omega}\|^4)\,. \tag{4.5}$$

(The above relation is easily determined by use of Taylor series expansions.) Thus, with respect to the orientation of the principal axes of the stress, the Hughes-Winget algorithm is second order accurate. □

*Stability analysis*

In this section, the hypoelastic algorithms are analyzed for stability with respect to a motion with constant spin. Without loss of generality the analysis is performed for a 2-D problem. An identical result holds in 3-D but involves a higher dimensional eigenproblem which does not provide additional understanding.

For the purposes of the stability analysis it is convenient to write the stress tensor in vector form where

$$\boldsymbol{\sigma} = \begin{pmatrix} \sigma_{11} \\ \sigma_{12} \\ \sqrt{2}\sigma_{12} \end{pmatrix}\,. \tag{4.6}$$

If one now considers a motion with constant $\boldsymbol{\Omega}$ of norm $\alpha$, then the equation for the material time rate of change of the stress can be expressed as

$$\dot{\boldsymbol{\sigma}} + \boldsymbol{A}\boldsymbol{\sigma} = \boldsymbol{f}\,, \tag{4.7}$$

where $\boldsymbol{f} = \mathbb{C}\colon \boldsymbol{d}$ in vector form and

$$\boldsymbol{A} = \begin{bmatrix} 0 & 0 & \sqrt{2}\alpha \\ 0 & 0 & -\sqrt{2}\alpha \\ -\sqrt{2}\alpha & \sqrt{2}\alpha & 0 \end{bmatrix}. \tag{4.8}$$

The eigenvalues of the matrix $\boldsymbol{A}$ are $\{0, \pm 2\alpha i\}$ where $i$ is the imaginary unit. This indicates that the homogeneous solutions to (4.7) are oscillatory or unchanging. The zero eigenvalue corresponds to the pressure of the stress tensor which is unaffected by rigid-body rotation.

The application of ALGO1 to (4.7) results in the following expression

$$\boldsymbol{\sigma}_{n+1} = \boldsymbol{\sigma}_n - \Delta t \boldsymbol{A}_{n+1/2}\boldsymbol{\sigma}_n + \Delta t \boldsymbol{f}_{n+1/2}\,, \tag{4.9}$$

**Remark 4.4.**
It is easily seen that ALGO1 is midpoint on the kinematics of (4.7) but only forward Euler on the stress part of the expression, as was alluded to in §2. □

For convenience in the remainder $\boldsymbol{d}$ will be assumed zero. Under the given assumptions,

$$\boldsymbol{\sigma}_{n+1} = \begin{bmatrix} 1 & 0 & -\Delta t\sqrt{2}\alpha \\ 0 & 1 & \Delta t\sqrt{2}\alpha \\ \Delta t\sqrt{2}\alpha & -\Delta t\sqrt{2}\alpha & 1 \end{bmatrix} \boldsymbol{\sigma}_n\,, \tag{4.10}$$

where the matrix in (4.10) is recognized to be the amplification matrix for the algorithm. Stability requires that the spectral radius of the amplification matrix $\rho \leq 1$, where $\rho$ is the maximum magnitude of the eigenvalues of the amplification matrix. For the case at hand, the eigenvalues are $\{1, 1 \pm 2\alpha\Delta t i\}$ and

$$\rho = \sqrt{1 + 4\alpha^2\Delta t^2} > 1\,. \tag{4.11}$$

Thus, one concludes that *ALGO1 is UNCONDITIONALLY UNSTABLE in the presence of rotations.*

Application of ALGO2 to (4.7) results in

$$\boldsymbol{\sigma}_{n+1} = \begin{bmatrix} 1-\alpha^2\Delta t^2 & \alpha^2\Delta t^2 & -\Delta t\sqrt{2}\alpha \\ \alpha^2\Delta t^2 & 1-\alpha^2\Delta t^2 & \Delta t\sqrt{2}\alpha \\ \Delta t\sqrt{2}\alpha & -\Delta t\sqrt{2}\alpha & 1-\alpha^2\Delta t^2 \end{bmatrix} \boldsymbol{\sigma}_n\,. \tag{4.12}$$

The eigenvalues of this amplification matrix are $\{1, (1 - 2\alpha^2\Delta t^2) \pm 2\sqrt{2}\alpha\Delta t i\}$ and the spectral radius

$$\rho = \sqrt{1 + 4\alpha^4\Delta t^4} > 1\,. \tag{4.13}$$

Thus, *ALGO2 is UNCONDITIONALLY UNSTABLE in the presence of rotations.*

**Remark 4.5.**

The degree of instability in these two algorithms is in a practical sense small since $\alpha\Delta t$ is usually much less than 1. Nonetheless, it is still finite and in the presence of large rotations ALGO1 possesses a much stronger instability than ALGO2. Thus ALGO1 will diverge before ALGO2. Quantitative evidence to this effect is given in §5. □

Application of the Hughes-Winget or exponential map algorithm to (4.7) results in

$$\boldsymbol{\sigma}_{n+1} = \begin{bmatrix} \cos^2\theta & \sin^2\theta & -\sqrt{2}\cos\theta\sin\theta \\ \sin^2\theta & \cos^2\theta & \sqrt{2}\cos\theta\sin\theta \\ \sqrt{2}\cos\theta\sin\theta & -\sqrt{2}\cos\theta\sin\theta & \cos^2\theta - \sin^2\theta \end{bmatrix} \boldsymbol{\sigma}_n \,, \tag{4.14}$$

where the angle $\theta = \alpha\Delta t$ for the exponential map algorithm and $\theta = \alpha\Delta t + \delta$, where $\delta \sim O(\alpha^3\Delta t^3)$, for the Hughes-Winget algorithm. The eigenvalues for this amplification matrix are $\{1, (\cos^2\theta - \sin^2\theta) \pm i\sqrt{1 - (\cos^2\theta - \sin^2\theta)^2}\}$. The spectral radius

$$\rho = 1 \,. \tag{4.15}$$

Thus, these two algorithms are unconditionally stable.

**Remark 4.6.**

All the stability results carry over to 3-D where one must solve a six-dimensional eigenvalue problem. Note that in this case 1 becomes a repeated eigenvalue for all algorithms but with linearly independent eigenvectors. □

## §5. Illustrations

To illustrate the behavior of the algorithms analyzed above in applications, two simple problems are considered. The first involves the calculation of the stress at a single point in a body under going rigid-body rotation with a given initial stress. The second involves the simulation of a square slab that is impulsively loaded in order to induce a large rigid-body component to the motion.

*Single stress point example*

Consider a point in a body undergoing a rigid-body rotation ($\boldsymbol{d} = 0$) of roughly 600 rad/s corresponding to a spin tensor

$$\boldsymbol{\Omega} = \begin{bmatrix} 0 & 346 & -346 \\ -346 & 0 & 346 \\ 346 & -346 & 0 \end{bmatrix} . \tag{5.1}$$

Assume at a given instant in time that the Cauchy stress at the point is given by

$$\boldsymbol{\sigma} = \begin{bmatrix} 1 & 4 & 6 \\ 4 & 2 & 5 \\ 6 & 5 & 3 \end{bmatrix} . \tag{5.2}$$

The invariants of this stress state are $\mathrm{tr}\,\boldsymbol{\sigma} = 6$, $\frac{1}{2}[(\mathrm{tr}\,\boldsymbol{\sigma})^2 - \mathrm{tr}\,\boldsymbol{\sigma}^2] = -66$ , and $\det[\boldsymbol{\sigma}] = 101$.

Using the Hughes-Winget or the exponential map algorithm to update the stress exactly preserves the three invariants when using an invariant preserving matrix multiplication routine. The Saint Venant-Kirchhoff model also exactly preserves the invariants. These statements hold regardless of the time step size. For ALGO1 and ALGO2 the values of the invariants are plotted in Fig. 5.1 as a function of time step, where $\Delta t = 5 \times 10^{-6}$ s. As can be seen from the figure, ALGO1 produces large errors in the second and third invariants while ALGO2 appears exact. The error in ALGO2 is undetectable on the scale shown; it occurs in the 14th significant digit for the first invariant, in the 7th significant digit for the second invariant, and in the 6th significant digit for the third invariant when double precision variables are used. The drift in both algorithms is a combination of accuracy error and instability.

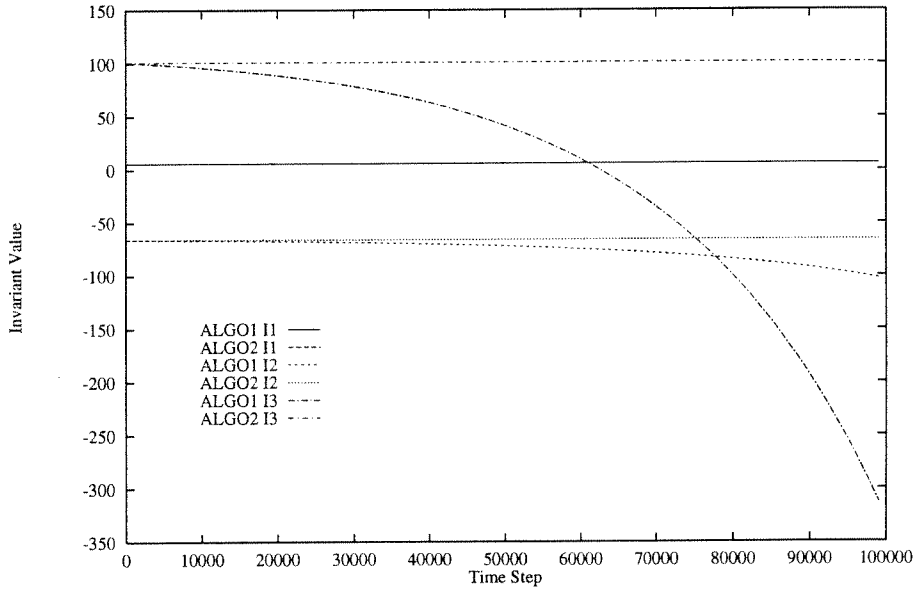


**FIGURE 5.1.** Comparison of ALGO1 and ALGO2 for the preservation of the stress invariants. In the figure legend I1 denotes the first invariant, I2 the second, and I3 the third. Note, that for I1 the two curves lie on top of each other.

**Remark 5.1.**

It is clear that even though ALGO2 is also unconditionally unstable, its performance is superior to ALGO1. □

*Spinning Square*

In this example, the motion of a slab spinning about its center is considered. The geometry under consideration is shown in Fig. 5.2. The edge lengths of the body are $\sqrt{2}$ m and the thickness is 0.5 m. The loads are applied in the plane of the slab and

are linearly ramped from a value of zero to $3 \times 10^{10}$ N in 20 $\mu$s and then back down to zero in 20 $\mu$s. This causes the slab to vibrate and spin about the 3-axis with an angular velocity of roughly 785 rad/s. The density of the slab is taken as 7850 kg/m$^3$ and the rank-4 constitutive tensor is assumed to be of the form $\mathbb{C} = 2\mu\mathbb{I} + \lambda \mathbf{1} \otimes \mathbf{1}$. The constant $\mu = 100 \times 10^9$ MPa and $\lambda = 0$. The body itself is discretized into 16 fully integrated 8-node bricks as shown in Fig. 5.2. In the simulation of the motion, no numerical damping is employed and a time step of $\Delta t = 5$ $\mu$s is employed. This is well below the Courant time step limit of 70 $\mu$s.

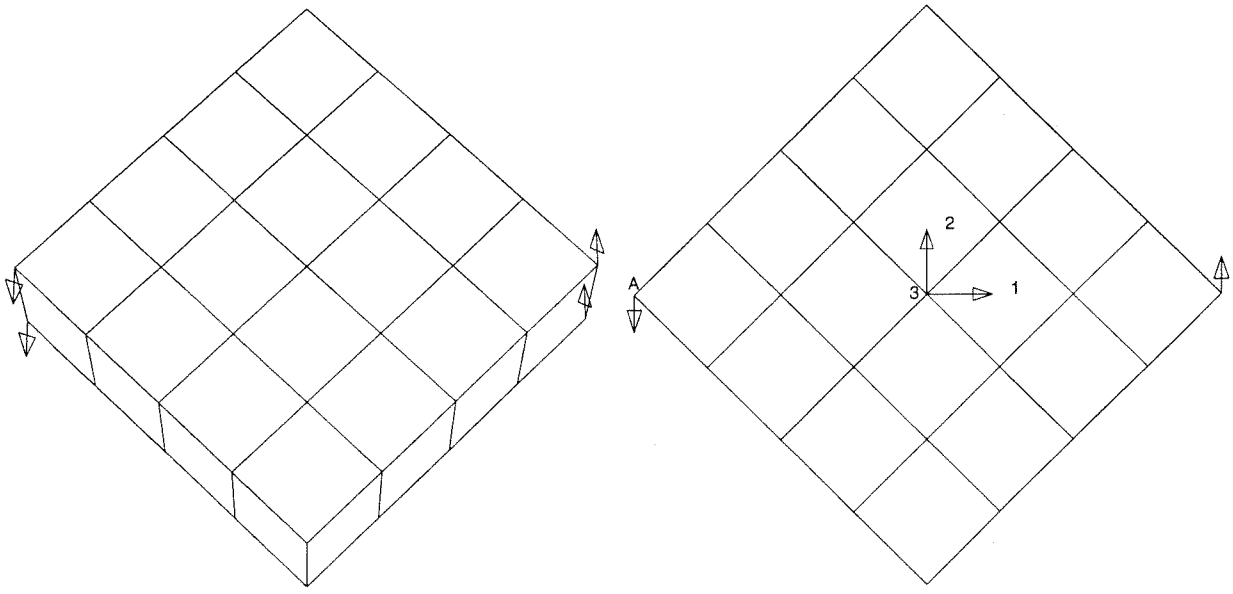


**FIGURE 5.2.** Geometry and loading of spinning slab. (left) isometric view, (right) top view.

Shown in Fig. 5.3 is the 1-displacement of point A [see Fig 5.2(right)] for all 4 hypoelastic formulations and the hyperelastic formulation. The hypoelastic formulations all produce virtually identical time history traces. The primary difference between the algorithms is the duration of the simulation before the global finite element calculation becomes unstable. Indicated in Fig 5.3 by the arrows are the times at which the various algorithms cause the global calculation to terminate.

**Remark 5.2.**

Use of ALGO2 increases the possible duration of simulation by 59% over ALGO1. The Hughes-Winget algorithm increases the possible duration of simulation by 16% over ALGO2. And the use of the exponential map algorithm increases the possible duration of simulation by 9% over the Hughes-Winget algorithm. □

**Remark 5.3.**

Another recent proposal similar in form to the ones presented here is the algorithm of Rashid [10]. This algorithm utilizes higher order kinematics than those presented

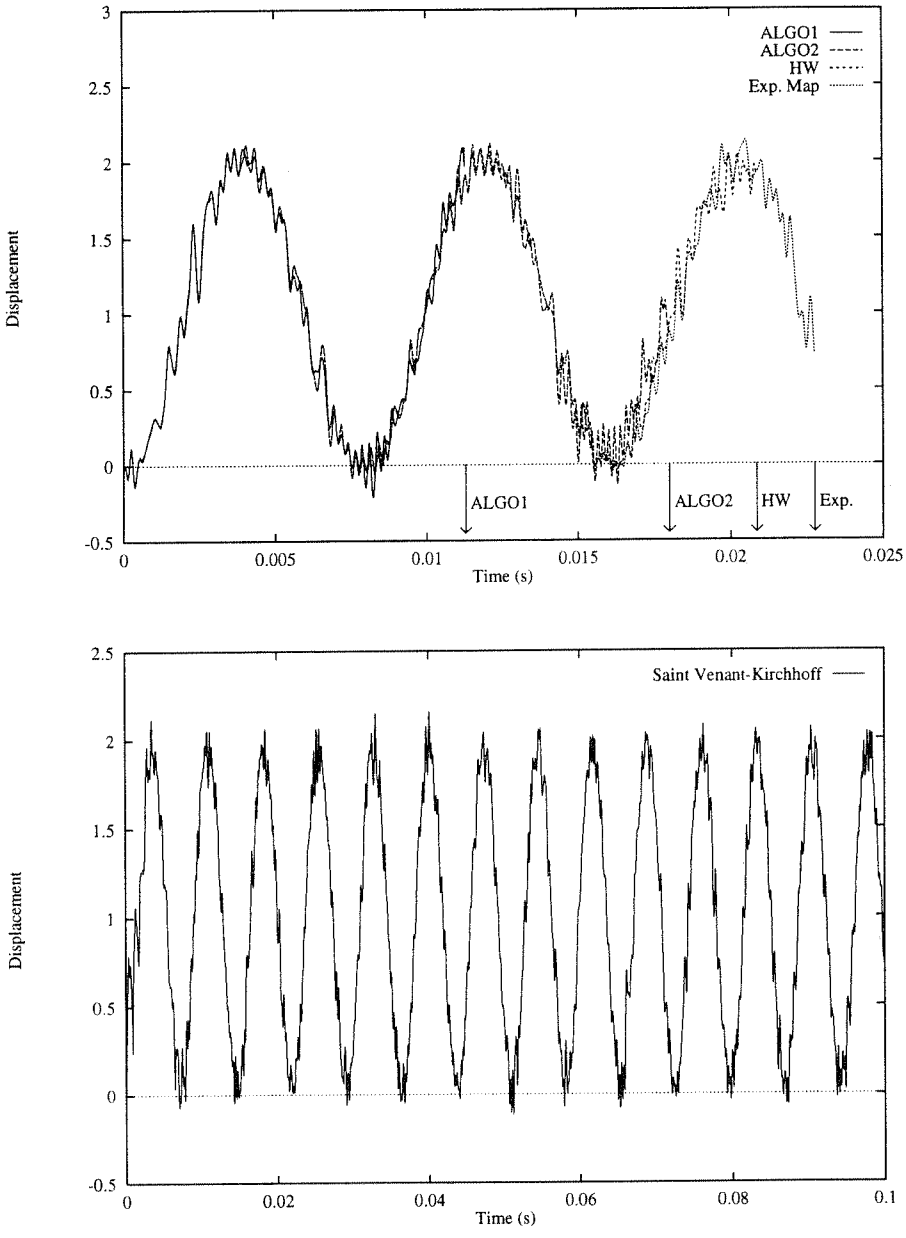


**FIGURE 5.3.** Displacement time history traces. (top) Hypoelastic algorithms, (bottom) Hyperelastic algorithm.

to reduce the coupling error during simultaneous rotation and stretching; see [10] for details. Nonetheless, it shows similar behavior for the problem at hand. Overall the use of this algorithm increases the possible duration by 11% over ALGO2 (without the use of "pre-conditioning"). □

**Remark 5.4.**

Also shown in Fig. 5.3 is the displacement of point A when the Saint Venant-Kirchhoff

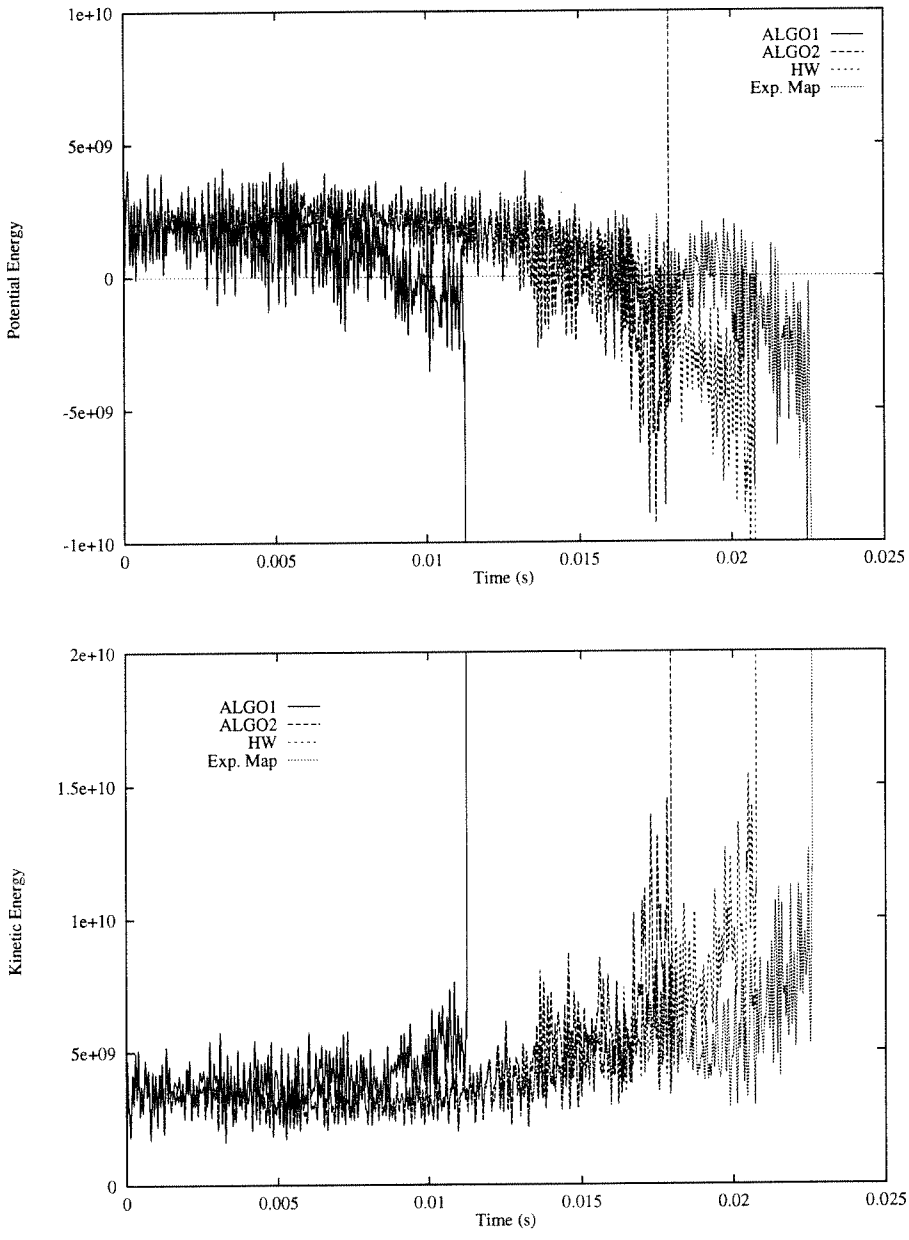


**FIGURE 5.4.** Energy time history traces for the slab using the hypoelastic algorithms. (top) potential energy , (bottom) kinetic energy.

model is used (with the same properties). The time history trace is shown up to 0.01 s. It is noted that the simulation shows no signs of instability and in fact has been continued past 5.0 s. □

The source of the global instability of the hypoelastic simulations can be seen from the time histories of the slab's total potential and kinetic energies; see Fig. 5.4. Note that for the calculation of the total potential energy the expression $\int_V \boldsymbol{\sigma}\colon \boldsymbol{d}$ is incrementally

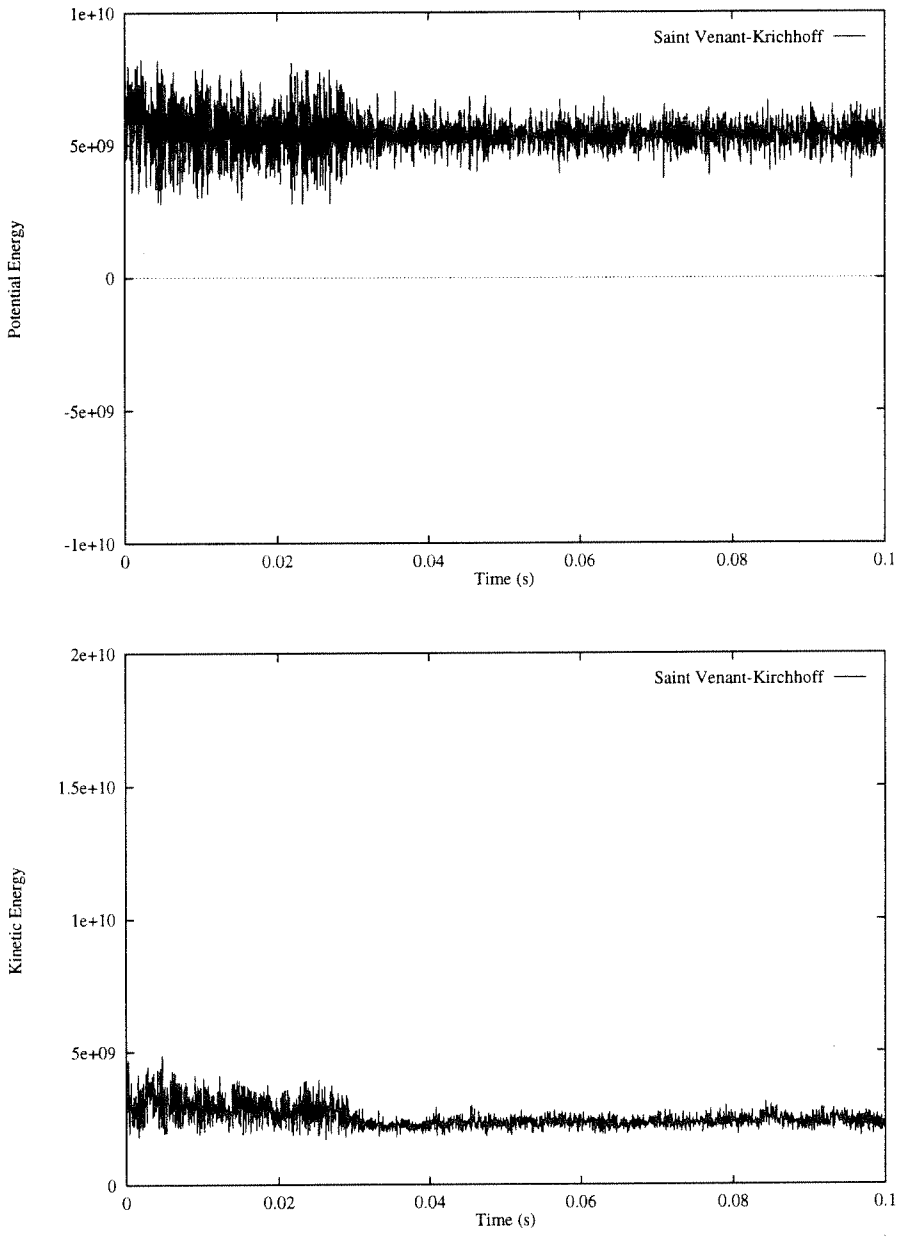


**FIGURE 5.5.** Energy time history traces for the slab using the Saint Venant-Kirchhoff model. (right) potential energy , (left) kinetic energy.

integrated in time using a mid-point rule for the hypoelastic models since no closed-form expression exists for the material's strain energy density. The figure shows that the potential energy of the body decreases as time elapses. At the same time, since the global time stepping algorithm attempts to conserves energy, the kinetic energy increases; eventually the calculation becomes unstable.

**Remark 5.5.**

Note that the points of instability of the 4 hypoelastic algorithms can be drawn closer to each other by decreasing the time step size until the difference in the algorithms is reduced to machine precision. However, the instability most likely cannot be completely eliminated as hypoelasticity in general fails to have zero work in closed cycles; see [12, §99-101] and references therein. Note that the instability does not manifest itself in the hyperelastic calculation. The time histories of the energies for the Saint Venant-Kirchhoff model are shown in Fig 5.5; to aide in comparison to Fig 5.4 the same scales are utilized for the abscissae. □

## §6. Conclusions

This paper has presented an accuracy and stability analysis of several common algorithms and one new one for the integration of hypoelastic constitutive relations based upon the Jaumann rate. The primary conclusions are as follows:

1. The simplest algorithm (ALGO1) is first order objective and unconditionally unstable in the presence of rotations.
2. The next most complex algorithm (ALGO2) is second order objective and unconditionally unstable in the presence of rotations. The degree of instability is 2 powers less than that of ALGO1; see Eq. (4.13) versus Eq. (4.11).
3. The Hughes-Winget algorithm is incrementally objective, second order accurate with respect to incrementally rigid-body motions, and unconditionally stable.
4. The exponential map algorithm is incrementally objective, exact with respect to incrementally rigid-body motions, and unconditionally stable.
5. The inaccuracies and instabilities of the hypoelastic algorithms can cause premature global instabilities in finite element calculations. By "premature", it is noted that a consistent and stable approximations to hypoelasticity can lead to a global instability of a boundary value problem as was illustrated in §5. The likely cause of this is that with a constant expression for $\mathbb{C}$, the hypoelasticity formulation considered is incompatible with hyperelasticity except in restrictive circumstances [13]. Further, for hypoelastic materials that are not hyperelastic the contrapositive of Bernstein's Theorem IV [14, 12 §101] tells us that the work performed on such a body is NOT non-negative for all closed cycles. A conclusive proof that this state of affairs is the cause of the observed global instability of the boundary value problem in §5 is not available but it is certainly felt to be a contributing factor given that the hyperelastic calculation shows no signs of instability.
6. In terms of the cost of the rotational update of the stress, viz. the construction of $\boldsymbol{Q}$ and the update $\boldsymbol{Q}\boldsymbol{\sigma}\boldsymbol{Q}^T$, ALGO1 requires 15 multiplies and 18 additions, ALGO2 requires 60 multiplies and 54 additions, the Hughes-Winget can be computed in 105 multiplies, 1 divide, and 45 additions, and the exponential map can be performed in 107 multiplies, 2 divides, 44 additions, 1 square-root, and 2 trigonometric evaluations.

The numbers for the Hughes-Winget and exponential map algorithms are not necessarily optimal and do not take into account invariant preserving matrix multiplication. A similar (non-optimal) count for the Rashid algorithm indicates 147 multiplies, 70 additions, 5 divides, and 2 square-roots.

## §7. Acknowledgments

The author wishes to thank Dr. E. Zywicz of the Lawrence Livermore National Laboratory for his continued interest and support in this research. Acknowledgment is also do to Mr. A. Guzman for programming ALGO1 and ALGO2 in the finite element code FEAP which was graciously made available by Prof. R.L. Taylor of the University of California at Berkeley.

## §8. References

[1] HALLQUIST, J.O. *Theoretical Manual for DYNA3D*, Lawrence Livermore National Laboratory, UCID-19401 (1983).

[2] JOHNSON, G.C. & BAMMANN, D.J. "A Discussion of Stress Rates in Finite Deformation Problems," *Int. J. Solids Struc.* **20**, 725-737 (1984).

[3] FLANAGAN, D.P. & TAYLOR, L.M. "An Accurate Numerical Algorithm for Stress Integration with Finite Rotations," *Comp. Meth. Appl. Mech. Engng.* **62**, 305-320 (1987).

[4] HIBBITT, KARLSSON, & SORENSEN, INC. *ABAQUS/Standard Theory Manual* (1994).

[5] SIMO, J.C. & HUGHES, T.J.R. *Elastoplasticity and Viscoplasticity, Computational Aspects*, Springer-Verlag (in press 1996).

[6] HUGHES, T.J.R. *The Finite Element Method*, Prentice Hall, Englewood Cliffs, NJ (1987).

[7] HUGHES, T.J.R. & WINGET, J. "Finite Rotation Effects in Numerical Integration of Rate Constitutive Equations Arising in Large-Deformation Analysis," *Int. J. Numer. Meth. Eng.* **15**, 1862-1867 (1980).

[8] GOLDSTEIN, H. *Classical Mechanics*, 2nd Edition, Addision-Wesley, Reading, MA (1981).

[9] LEWIS, D. & SIMO, J.C. "Conserving Algorithms for the Dynamics of Hamiltonian Systems on Lie Groups," *J. Nonlin. Sci.* **4**, 253-299 (1994).

[10] RASHID, M.M. "Incremental Kinematics for Finite Element Applications," *Int. J. Numer. Meth. Eng.* **36**, 3937-3956 (1993).

[11] GURTIN, M.E. *An Introduction to Continuum Mechanics*, Academic Press, Orlando (1981).

[12] TRUESDELL, C. & NOLL, W. *The Non-Linear Field Theories of Mechanics*, 2nd Edition, Springer-Verlag, Berlin (1992).

[13] SIMO, J.C. & PISTER, K.S. "Remarks on Rate Constitutive Equations for Finite Deformation Problems: Computational Implications," *Comp. Meth. Appl. Mech. Engng.* **46**, 201-215 (1987).

[14] BERNSTEIN, B. "Hypo-Elasticity and Elasticity," *Arch. Rat. Mech. Anal.* **6**, 89-104 (1960).